HHS Public Access

Author manuscript

Biochemistry. Author manuscript; available in PMC 2020 October 22.

Published in final edited form as:

Biochemistry. 2017 February 28; 56(8): 1151–1162. doi:10.1021/acs.biochem.6b01056.

Interaction of Zika Virus Envelope Protein with Glycosaminoglycans

So Young Kim[†], **Jing Zhao**[‡], **Xinyue Liu**[‡], **Keith Fraser**[§], **Lei Lin**[‡], **Xing Zhang**[‡], **Fuming Zhang**[*,‖], **Jonathan S. Dordick**[†,§,‖,⊥], **Robert J. Linhardt**[*,†,‡,§,‖,⊥]

[†]Biochemistry and Biophysics Graduate Program, Center for Biotechnology and Interdisciplinary Studies, Rensselaer Polytechnic Institute, Troy, New York 12180, United States

[‡]Department of Chemistry and Chemical Biology, Troy, New York 12180, United States

[§]Department of Biological Science, Center for Biotechnology and Interdisciplinary Studies, Rensselaer Polytechnic Institute, Troy, New York 12180, United States

[‖]Department of Chemical and Biological Engineering, Troy, New York 12180, United States

[⊥]Biomedical Engineering, Center for Biotechnology and Interdisciplinary Studies, Rensselaer Polytechnic Institute, Troy, New York 12180, United States

Abstract

In February 2016, the World Health Organization declared a Public Health Emergency of International Concern on Zika Virus (ZIKV), because of its association with severe fetal anomalies of congenitally infected humans. This has led to urgent efforts by academic, federal, and industry research groups to improve our understanding of the pathogenesis of ZIKV and to develop detection methods, therapeutic strategies, and vaccines. Although we still do not have the entire picture of the pathogenesis of ZIKV, extensive research has been conducted on related pathogenic flaviviruses (i.e., dengue virus, West Nile virus, and yellow fever virus). Binding to glycosaminoglycans (GAGs) through its envelope protein is the first step in successful host cell invasion of dengue virus. In this study, we examined ZIKV envelope protein (ZIKV E) binding to GAGs in a real time interaction study using surface plasmon resonance (SPR) to explore the role of GAGs in host cell entry of ZIKV into placenta and brain. ZIKV E strongly binds (K_D = 443 nM) pharmaceutical heparin (HP), a highly sulfated GAG, and binds with lower avidity to less sulfated GAGs, suggesting that the ZIKV E–GAG interaction may be electrostatically driven. Using SPR competition assays with various chain length HP oligosaccharides (from 4 to 18 saccharide units in length), we observed that ZIKV E preferentially binds to longer HP oligosaccharides (with 8–18 saccharides). Next, we examined GAGs prepared from human

[*]**Corresponding Authors** Department of Chemistry and Chemical Biology, Center for Biotechnology and Interdisciplinary Studies, Rensselaer Polytechnic Institute, Troy, NY 12180. zhangf2@rpi.edu. Telephone: (518) 276-3404. Fax: (518) 276-3405. linhar@rpi.edu.

Supporting Information

The Supporting Information is available free of charge on the ACS Publications website at DOI: 10.1021/acs.biochem.6b01056. Multiple-sequence alignment (MSA) of flavivirus envelope proteins generated using MSAviewer and a BLOSUM62 scoring matrix, PAGE analysis of the HS decasaccharide library used in the “fishing” experiment, and instrumental error in analysis of HS and CS standards (PDF)

The authors declare no competing financial interest.

placentas to determine if they bound ZIKV E, possibly mediating placental cell invasion of ZIKV. Compositional analysis of these GAGs as well as SPR binding studies showed that both chondroitin sulfate and heparan sulfate GAGs, present on the placenta, showed low-micromolar interactions with ZIKV E. Both porcine brain CS and HS also showed micromolar binding with ZIKV E. Moreover, heparan sulfate with a higher TriS content, the dominant repeating unit of HP, shows a high affinity for ZIKV E. These results suggest that GAGs may be utilized as attachment factors for host cell entry of Zika virus as they do in other pathogenic flaviviruses. They may also assist us in advancing our understanding of the pathogenesis of ZIKV and guide us in designing therapeutics to combat ZIKV with more insight.

Graphical Abstract

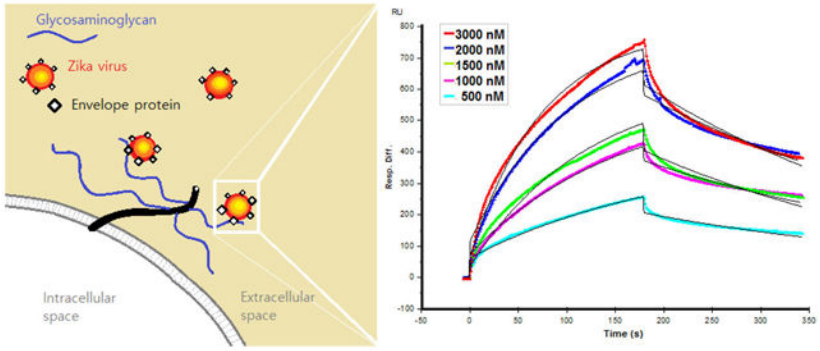

Mosquito-borne infectious diseases annually cause several million deaths and hundreds of millions of cases.[1] The malaria parasite puts 40% of the global population at risk and causes 3 million deaths each year. The range of arboviruses, also transmitted through insect vectors, is also increasing because of global warming. Dengue virus (DENV) has been considered to be the world's most dangerous mosquito-borne flavivirus disease, putting 2.5 billion people at risk of infection and resulting in 20 million cases each year. In February 2016, Zika virus (ZIKV) officially joined this list when the World Health Organization (WHO) declared a Public Health Emergency of International Concern for ZIKV's ability to cross the placental barrier and cause severe fetal anomalies in pregnant women.[2] First discovered in 1947, ZIKV is an enveloped, single-stranded RNA flavivirus and was known as a benign virus until microcephaly cases were reported in a 2015 outbreak in Brazil.[3] In healthy adults, ZIKV causes mostly mild symptoms such as fever, rash, and joint pain and is cleared out of the system in 1–2 weeks with the exception of a rare case of Guillain-Barre syndrome.[4,5] Congenital ZIKV infection, however, causes various fetal anomalies in the brain and other organs.[6-9] The current ZIKV outbreak to date has caused nearly 2500 reported congenital syndromes worldwide, with the highest occurrence in Brazil and the Caribbean.[10] Nearly 4000 ZIKV infections in pregnant women were reported in the United States and U.S. territories, and five pregnancies were lost due to ZIKV infection.[11] Most ZIKV cases in the United States were originally thought to be due to traveling in Brazil and the Caribbean; however, recent reports of local mosquito-borne ZIKV infection in Florida demonstrate that is no longer the case.

Since the WHO officially declared ZIKV a global threat to public health, there has been an intensified effort to understand the pathogenesis of ZIKV infection, particularly how ZIKV crosses the placental barrier. ZIKV infection can be transmitted through mosquito bites, congenitally, sexually, and through bodily fluids.[12-17] *In vitro* studies identified permissive cell types to ZIKV, such as human dermal fibroblasts, epidermal keratinocytes, and immature dendritic cells.[18] Human cortical neural progenitors also have been identified as the cell type ZIKV targets in the brain, and it has been determined that microcephaly may be due to neural cell death eventually causing microcephaly.[19,20] Recently, a study of brain scans and ultrasound images of 45 Brazilian babies who were congenitally infected with ZIKV suggests that ZIKV can disrupt brain development as well as reduce brain size.[21] *In vivo* studies show that a lack of interferon γ can enhance ZIKV infection and also cause microcephaly in a mouse model.[22,23] The AXL tyrosine kinase receptor has been identified as a primary receptor for host cell entry.[18,24] Two DNA vaccines entered Phase I clinical trials in August 2016; however, it may take several years to prepare safe and effective vaccines.[25]

Even though we have many pieces of the puzzle of ZIKV's pathogenesis, we still lack a basic understanding of how ZIKV enters host cells. Host cell invasion of other pathogenic flaviviruses, however, has been extensively studied and may guide us in understanding ZIKV's pathogenesis. The initial step in host cell invasion of various flaviviruses is to bind and concentrate on host cells and gain access to surface receptors.[26-43] The flaviviruses then enter the host cells through a clathrin-mediated endocytosis mechanism, and their envelope proteins go through conformational changes resulting in membrane fusion and release of the viral genome.[44-46] For example, all pathogenic flaviviruses, such as DENV, yellow fever virus (YFV), Japanese encephalitis virus (JEV), tick-borne encephalitis virus (TBEV), Murray encephalitis virus (MEV), and West Nile virus (WNV), utilize negatively charged glycosaminoglycans (GAGs) present on the host cell surface as attachment factors, while their other primary receptors vary.[47-52] In addition, pathogens that cause congenital anomalies, such as *Plasmodium falciparum,* cytomegalovirus, human immunodeficiency virus, and herpes simplex virus, also utilize GAGs within the host cell glycocalyx as attachment factors.[53-56] Many bacterial, parasitic, and viral infectious diseases similarly utilize GAGs as a coreceptor for successful host cell invasion.[57] GAGs are anionic, linear polysaccharides composed of repeating disaccharide units, located on the surface of cells and in the extracellular matrix (ECM). GAGs are involved in many biological processes such as cell adhesion, cell migration, tissue repair, ECM assembly, inflammation, and pathogenesis.[58]

The crystal structure of ZIKV envelope protein (ZIKV E) closely resembles that of other flaviviruses, such as WNV, JEV, and DENV (Figure 1). While crystal structures of ZIKV and other flavivirus envelope proteins have been previously investigated, cocrystallization in complex with GAGs has not been reported.[59-63] Many of these previous studies took a mutagenesis approach to identify the two putative noncontiguous GAG-binding regions within flavivirus envelope proteins. The binding regions are located at similar positions in the envelope proteins of ZIKV, DENV, and other flaviviruses.[47,64-68] Examining the sequence and structure of these GAG-binding regions within the envelope proteins, in comparison with those for ZIKV E, led us to hypothesize that ZIKV E could also bind to

host cell surface GAGs as an initial step in invasion (Figure 1 and Figure S1). In this study, we tested the interactions between ZIKV E and various GAGs using a surface plasmon resonance (SPR) binding assay. We also used SPR competition assays to understand the chain length requirements for ZIKV E–GAG interaction. We next isolated GAGs from human placenta and from porcine brain to understand their GAG composition and determined their specificity and interactions with ZIKV E.

EXPERIMENTAL PROCEDURES

Materials.

Three human placentas were purchased from Cardinal Biologicals (Tyler, TX). Recombinant Zika virus envelope protein was from MyBioSource, Inc. (San Diego, CA). Porcine intestinal heparin (HP), 16 kDa, and porcine intestinal heparan sulfate (HS), 12 kDa, were purchased from Celsus Laboratories (Cincinnati, OH). Porcine rib cartilage chondroitin sulfate type A (CSA), 20 kDa, porcine intestinal chondroitin sulfate type B (CSB), 30 kDa, and shark cartilage chondroitin sulfate type C (CSC), 20 kDa, were purchased from Sigma (St. Louis, MO). Whale cartilage chondroitin sulfate type D (CSD), 20 kDa, and squid cartilage chondroitin sulfate type E (CSE), 20 kDa, were purchased from Seikagaku (Tokyo, Japan). Keratan sulfate (KS), 14.3 kDa, was isolated from bovine cornea.[69] HP oligosaccharides, including tetrasaccharide [degree of polymerization 4 (dp4)], hexasaccharide (dp6), octasaccharide (dp8), decasaccharide (dp10), dodecasaccharide (dp12), tetradecasaccharide (dp14), hexadecasaccharide (dp16), and octadecasaccharide (dp18), were prepared using controlled partial heparinase 1 treatment of bovine lung HP (Sigma) followed by size fractionation.[70] Figure 2A illustrates chemical structures of these GAGs and HP oligosaccharides. The HS decasaccharide library for the “fishing” experiments was prepared by enzymatic depolymerization using the combination heparin lyase I, II, and III digestion and fractionation on a Bio-Gel P-6 column. The chain length of the HS decasaccharide library was confirmed by polyacrylamide gel electrophoresis (PAGE) analysis (Figure S2). Streptavidin (SA) sensor chips were purchased from GE healthcare (Pittsburgh, PA). SPR measurements were performed on a BIAcore 3000 system operated with BIAcore 3000 control and BIAevaluation version 4.0.1 from GE healthcare.

Unsaturated disaccharide standards of CS (ΔUA-GalNAc, ΔUA-GalNAc4S, ΔUA-GalNAc6S, ΔUA2S-GalNAc, ΔUA2S-GalNAc4S, ΔUA2S-GalNAc6S, ΔUA-GalNAc4S6S, and ΔUA2S-GalNAc4S6S), unsaturated disaccharide standards of HS (ΔUA-GlcNAc, ΔUA-GlcNs, ΔUA-GlcNAc6S, ΔUA2S-GlcNAc, ΔUA2S-GlcNS, ΔUA-GlcNS6S, ΔUA2S-GlcNAc6S, and ΔUA2S-GlcNS6S), and an unsaturated disaccharide standard of HA (ΔUA-GlcNAc), where ΔUA is 4-deoxy-α-L-*threo*-hex-4-enopyranosyluronic acid, S is sulfo, and Ac is acetyl, were from Iduron. Actinase E was obtained from Kaken Biochemicals (Tokyo, Japan). Chondroitin lyase ABC from *Proteus vulgaris* was expressed in *Escherichia coli* in our laboratory. Recombinant Flavobacterial heparinase I, II, and III were expressed in our laboratory using *E. coli* strains that were gifts of J. Liu (University of North Carolina at Chapel Hill, Chapel Hill, NC).[71] 2-Aminoacridone (AMAC) and sodium cyanoborohydride ($NaCNBH_3$) were obtained from Sigma-Aldrich (St. Louis, MO). Amine-PEG3-biotin was purchased from Thermo Fisher Scientific (Waltham, MA). All other chemicals were of high-

performance liquid chromatography (HPLC) grade. Vivapure Q Mini H strong anion exchange spin columns were from Sartoriou Stedim Biotech (Bohemia, NY).

Extraction of Glycosaminoglycans from Human Placenta.

Tissues were thawed at 4 °C and rinsed with chilled phosphate-buffered saline (PBS). Placenta was dissected into three regions: cotyledon, chorionic plate, and umbilical cord (Figure 2B). Each region was lyophilized and cut into smaller pieces prior to defatting with acetone and being shaken at room temperature for 1 h. Once acetone was completely evaporated, the tissue was digested using Actinase E for 12–24 h. Completely digested tissues were lyophilized. Dry tissues were dissolved in 8 M urea and 2 wt % CHAPS {3-[(3-cholamidopropyl)dimethylammonio]-1-propanesulfonate} buffer, and GAGs were purified using MAXI H spin columns.[72] GAGs were desalted using 3 kDa molecular weight cutoff (MWCO) spin columns and lyophilized.

Digestion of GAG into CS and HS.

Lyophilized GAG samples were treated with a mixture of recombinant heparinase I, II, and III in digestion buffer (20 milliunits each per milligram of GAG in 50 mM ammonium acetate containing 2 mM calcium chloride adjusted to pH 7.0) at 37 °C for 5 h to prepare intact CS. The reaction was terminated when the mixture was placed in a 100 °C water bath for 5 min. The reaction mixture was cooled and spun down in 3 kDa columns to remove the HS disaccharide products. The retentate containing CS was collected from the spin column and lyophilized for SPR studies. The permeate (disaccharides) was collected and lyophilized for disaccharide analysis. The same protocol was applied to prepare intact HS except the sample was treated with chondroitinase ABC in place of heparinases.

AMAC Labeling.

The dried samples were labeled with AMAC (2-aminoacridone) by addition of 10 μL of 0.1 M AMAC in a DMSO/acetic acid solvent [17/3 (v/v)] and incubation at room temperature for 10 min, followed by addition of 10 μL of 1 M aqueous $NaBH_3CN$ and incubation for 1 h at 45 °C. A mixture containing all 17 disaccharide standards prepared at 12.5 ng/μL was similarly labeled with AMAC and used for each run as an external standard. A second mixture, containing eight HS disaccharide standards at 12.5 ng/μL, was used for disaccharide analysis in the “fishing” experiment. After the AMAC labeling reaction, the samples were centrifuged and each supernatant was recovered.

Disaccharide Analysis Using Liquid Chromatography and Mass Spectrometry (LC–MS).

LC–MS analyses were performed on an Agilent 1200 LC/MSD instrument (Agilent Technologies, Inc., Wilmington, DE) equipped with a 6300 ion trap and a binary pump. The LC column was an Agilent Poroshell 120 C18 column (2.7 μm, 3.0 mm × 150 mm). The column temperature was 45 °C. The flow rate was 150 μL/min. The mobile phases were 50 mM NH_4OAc in water (A) and methanol (B): gradient of 5 to 30% B from 0 to 20 min, 30 to 50% B from 20 to 30 min, 100% B from 30 to 40 min, and 5% B from 40 to 50 min. The MS parameters were electrospray in negative ionization mode with a skimmer potential of −40.0 V, a capillary exit of −40.0 V, and a source temperature of 350 °C. The mass range of

the spectrum was *m/z* 300–900. Nitrogen (8 L/min, 40 psi) was used as the drying and nebulizing gas.

Biotinylation of GAGs.

Purified GAGs, including HS and CS (2 mg), amine-PEG3-biotin (2 mg), and $NaCNBH_3$ (10 mg) were dissolved in 180 μL of H_2O, and 20 μL of acetic acid was added. The reaction mixture was heated at 70 °C for 24 h. After 24 h, an additional 10 mg of $NaCNBH_3$ was added to the reaction mixture and the mixture heated under the same conditions for an additional 24 h. After cooling to room temperature, the reaction mixture was desalted with a 3 kDa spin column, and the biotinylated GAGs were collected and lyophilized.

Immobilization of GAGs on a SPR Chip.

Biotinylated GAGs were immobilized on the carboxymethylated dextran streptavidin sensor chip. The sensor chip was conditioned with 1 M NaCl in 50 mM NaOH at a flow rate of 10 μL/min, and biotinylated GAGs (10 μL containing 2 μg of either biotinylated HS or CS) were then injected onto the flow channel. The control flow channel was prepared with a saturated solution of biotin. Successful immobilization was confirmed by observing a resonance unit (RU) of ≥100.[72]

Binding Assay for Assessing Interactions between ZIKV E and GAGs Using SPR.

Various concentrations of ZIKV E were prepared in HBS-EP buffer [0.01 M HEPES, 0.15 M NaCl, 3 mM EDTA, and 0.005% surfactant P20 (pH 7.4)] and used in these studies for the HP sensor chip (63, 125, 250, 500, and 1000 nM), for the placental GAG sensor chip (500, 1000, 1500, 2000, and 3000 nM), and for the porcine brain GAG sensor chip (1000, 2000, 3000, 4000, and 5000 nM). These concentrations were selected to give a strong RU response in the sensorgrams that were obtained. ZIKV E was injected over the surface of appropriate sensor chips at a flow rate of 30 μL/min. After sample injection, the surface of the sensor chip was dissociated by being washed with 90 μL of HBS-EP buffer, followed by washing with 30 μL of 2 M NaCl for regeneration. RU was monitored as a function of time (sensorgram) at 25 °C.

SPR Competition Assays To Inhibit Binding of ZIKV E to a HP Chip by Soluble HP Oligosaccharides and Soluble GAGs.

The HP-immobilized SA chip was used for this experiment. Recombinant ZIKV E (500 nM) was mixed with 2 μM HP oligosaccharides, including dp4–dp18, in HBS-EP buffer. A control experiment was performed with a mixture of ZIKV E and HBS-EP buffer. A mixture of ZIKV E with each HP oligosaccharide was injected over the surface of the HP-immobilized sensor chip at a flow rate of 30 μL/min. After each run, the dissociation and regeneration steps were performed. The same protocol was used for the competition assay of various GAGs, including HP, HS, CSA, CSB, CSC, CSD, CSE, and KS.

“Fishing” Experiment.

ZIKV E (30 μg) and 100 μg of the HS oligosaccharide library of dp 10 were each dissolved in 100 μL of 25 mM HBS-EP buffer [0.01 M HEPES, 0.15 M NaCl, 3 mM EDTA, and

0.005% surfactant P20 (pH7.4)], and the mixture was incubated at room temperature for 1 h. Nonbinding oligosaccharides were removed from the mixture using 10 kDa MWCO spin columns, and ZIKV E–HS oligosaccharide complexes retained in the spin column were washed three times with buffer and then subjected to LC–MS disaccharide compositional analysis.

RESULTS

Binding of ZIKV E to HP.

HP is abundantly biosynthesized in mucosal tissues of porcine intestinal and bovine lung tissues, but not generally present in the brain or placenta.[73] Electrostatic interaction is believed to be the main type of interaction between various flavivirus envelope proteins and GAGs, and HP is the most negatively charged GAG.[47] On this basis, we began by examining interaction of HP with ZIKV E by a real time SPR binding assay to determine binding kinetics. ZIKV E (63–1000 nM) was injected over the surface of a HP-immobilized sensor chip. Sensorgrams were fit globally to generate kinetic constants under a standard Langmuir kinetic model (Figure 3), and observed kinetic constants k_a, k_d, and K_D were 9.67×10^3 M^{-1} s^{-1}, 4.28×10^{-3} s^{-1}, and 443 nM, respectively (Table 1). The sensorgrams obtained showed the RU increased in a concentration-dependent manner.

ZIKV E Preferentially Binds to HP Oligosaccharides of Longer Chain Lengths.

In addition to electrostatic interactions, the chain length of GAGs has been shown to play an important role in efficient binding to envelope protein in closely related flaviviruses, such as DENV.[47] We performed a SPR competition assay to understand whether ZIKV E–HP binding requires a certain HP chain length. In these SPR competition assays, a mixture of ZIKV E and various HP oligosaccharides (dp4–dp18) was injected over the surface of a HP-immobilized sensor chip. RU, indicating binding affinity, was normalized on the basis of a ZIKV E–HBS buffer control. The level of ZIKV E–HP binding decreased with an increasing HP oligosaccharide chain length (Figure 4). The results show that the minimum chain length for binding was an octasaccharide (8-mer). The level of inhibition increased with increasing HP oligosaccharide chain length to 89.2% (±0.9%) for octadecasaccharide (dp18).

Preferential Binding of ZIKV Envelope Protein to Specific GAG Structures.

In previously studied infectious diseases, an efficient GAG–protein interaction required GAGs with specific saccharide sequence and sulfation patterns.[57,74-77] We screened various GAGs for their ability to inhibit ZIKV E–HP interaction using a SPR competition assay to test whether the ZIKV E–GAG interaction exhibits specificity. A mixture of ZIKV E and various natural GAGs, including HP, HS, CSA, CSB, CSC, CSD, CSE, and KS, was injected over the surface of the HP-immobilized sensor chip. The stronger affinity of a particular GAG for ZIKV E, the greater the inhibition of the interaction of HP with ZIKV E observed. HP showed the strongest inhibition level of 95.2% (±0.3), followed by CSE of 79.2% (±0.9), CSB of 71.6% (±1.2), HS of 57.1% (±1.6), KS of 41.4% (±2.1), CSD of 65.2% (±3.0), CSA of 19.1% (±8.3), and CSC of 8.2% (±0.4) (Figure 5).

Disaccharide Analysis of Placental GAGs.

Next, GAGs were isolated from three regions of human placenta tissues, cotyledon, chorionic plate, and umbilical cord (Figure 2B) via a procedure previously established in our laboratory.[72] The main steps of isolation of GAGs from placental tissues include defatting, proteolysis, and ion exchange column purification. GAG samples were treated with appropriate enzymes, heparinases I, II, and III, affording CS, and chondroitinase ABC, affording HS. CS and HS were then further purified using 3 kDa spin columns. The disaccharide compositions of AMAC-labeled total GAG, CS, and HS from three different regions of placenta were analyzed by LC–MS. The percent compositions of total GAGs comprising CS, HS, and hyaluronan (HA) were 69.87% (±1.84%), 15.38% (±7.89%), and 14.75% (±9.26%), respectively (Table 2). The dominant forms of CS found were 4S (69%) and 6S (27.1%) (Table 3). Thus, the dominant forms of CS in human placenta were identified as CSA and/or CSB (69%), followed by CSC (27.1%). Finally, the most abundant types of HS were found to be 0S (50.7%), NS (24.9%), and NS2S (13.3%). The chemical structures of various repeating units of CS and HS are illustrated in Figure 2A.

Binding of ZIKV Envelope Protein to Human Placental CS and Human Placental HS.

We next performed a SPR binding assay to determine the binding affinity of ZIKV E–placental CS and ZIKV E–placental HS interactions to investigate if placental GAGs may mediate host cell entry of ZIKV in placenta. ZIKV E (500–3000 nM) was injected over the surface of placental CS- and placental HS-immobilized sensor chips. Sensorgrams that were generated fit the Langmuir kinetics very well, and kinetic constants were obtained (Figure 6 and Table 1). Kinetic constants k_a, k_d, and K_D for placental CS were 4.10×10^3 M^{-1} s^{-1}, 2.70×10^{-3} s^{-1}, and 658 nM, respectively (Table 1). Although the kinetic constants were also calculated for placental HS, sensorgrams did not provide a good fit for concentration-dependent binding (not shown).

Binding of ZIKV Envelope Protein to Porcine Brain CS and Brain HS.

We next determined the binding affinity of ZIKV E for porcine brain GAGs using a SPR kinetic assay to investigate if surface GAGs might mediate host cell entry of ZIKV into the brain. Porcine brain CS and HS, previously isolated in our laboratory, were immobilized on the surface of the SA sensor chip.[78] The most abundant types of CS were 4S (CSA and/or CSB, ~80%), 6S (CSC, ~7%), and 0S (~8%), whereas major HS types were 0S (60%), TriS (25%), NS2S (13%), and NS6S (3%). ZIKV E (1000–5000 nM) was injected over the surface of brain CS- and brain HS-immobilized sensor chips. Globally fit sensorgrams generated kinetic constants under a Langmuir kinetic model (Table 1). In contrast to the case of placental CS and placental HS, brain HS showed concentration-dependent binding much better than that of brain CS (sensorgrams not shown). R_{max} was approximately 350 RU for both brain CS and brain HS at the injected concentrations.

"Fishing" Experiment with HS Decasaccharides for Components Binding to ZIKV E with High Affinity.

We performed a "fishing" experiment to determine which component in a library of HS decasaccharides had a high affinity for ZIKV E. The library of HS decasaccharides contains

hundreds of individual decasaccharide components.[79] The HS decasaccharide library and ZIKV E were incubated together at room temperature for 1 h before being filtered through 10 kDa MWCO spin columns to remove unbound HS decasaccharides with low ZIKV E affinity. A control was performed in the absence of ZIKV E. The disaccharide compositions of HS decasaccharides retained in the spin column, in the control and experimental samples, were determined using LC–MS. Our results show that TriS (4.3%) and 6S (3.25%) were enhanced and 0S (−6.15%) was depleted in the high-affinity decasaccharides compared to the low-affinity control (Figure 7).

DISCUSSION

GAGs have been widely found to be the first interface between a host cell and various bacterial, parasitic, and viral pathogens.[57] They allow pathogens to attach to and concentrate themselves on the surface of host cells before interacting with other primary receptors that directly facilitate their entry into the host cells.[26-43] Interactions between GAGs and surface proteins of pathogens can occur through both specific and nonspecific mechanisms. For example, the main driving force for interactions between the surface GAGs on the host cell and envelope protein of DENV and other pathogenic flaviviruses is electrostatic interaction between the negative charge of GAGs and positive regions on the envelope proteins.[47] In addition, GAG–protein interactions also exhibit structural specificity where proteins bind to GAGs with certain saccharide sequences and lengths as well as GAG chains at specific positions in the proteoglycan.[47,53,81] Putative GAG-binding regions on the envelope proteins of pathogenic flaviviruses are located in the proximity of each other.[47,64-68] ZIKV E's sequential and structural similarity to envelope proteins of other flaviviruses on their GAG-binding regions motivated us to examine the role of GAGs in the pathogenesis of ZIKV.

Although HP is not present in significant amounts in either brain or placenta, it represents an excellent starting point for studying ZIKV E because HP is the most negatively charged GAG and HS-containing HP-like domains have been reported in various tissues. It is likely that the major driving force for pathogenic flavivirus envelope protein–GAG interaction is electrostatic interaction.[47] Nanomolar concentrations (63–1000 nM) of ZIKV E injected across the HP-immobilized sensor chip showed concentration-dependent sensorgrams (Figure 3). The resulting kinetic constants, determined under a Langmuir kinetic model (Table 1), showed a high-affinity interaction with ZIKV E (K_D = 443 nM), which is weaker than the interaction of DENV envelope protein with low-molecular weight heparin determined by isothermal titration calorimetry (ITC) (K_D = 15 nM).[47] Although SPR and solution-based ITC binding interaction methods can produce kinetic constants that are in agreement with each other, several factors, such as rotational entropic properties and the surface density of the immobilized ligand, may influence binding interactions.[80]

A closer look at sequence alignment and superimposed crystal structure of GAG-binding regions of DENV E and ZIKV E may provide an explanation for the differences observed in binding of GAG to DENV E and ZIKV E (Figure 1 and Figure S1). While the GAG-binding sites DENV E and ZIKV E appear to be highly homologous, there are some differences in basic residues on the surface structure. GAG-binding sites of some proteins can be predicted by Cardin-binding motifs, "XBBXBX" and "XBBBXXBX", where X is a hydropathic

residue and B is a basic residue, and basic residues, such as arginine and lysine, are responsible for GAG binding.[81] Unfortunately, not all GAG-binding proteins contain contiguous motifs responsible for GAG binding, and in the case of DENV E and ZIKV E, Cardin-binding motifs do not comprise their GAG-binding sites.[82] Hydrogen-bonding residues can also play a role in GAG–protein interaction, contributing to both binding strength and specificity.[83] The basic surface residues that we believe contribute to GAG binding in ZIKV E are within the same regions as reported for DENV E (Figure 1).[47] The first clusters of basic and hydrogen-bonding surface residues (Figure 1B, GAG-binding site I in Figure S1) in these envelope proteins are identical with the exception of three residues; in ZIKV E, these residues are R299, A311, and T313, while in DENV E, they are Q293, K305, and K307. In the second cluster of basic and hydrogen-bonding residues (Figure 1C, GAG-binding site II in Figure S1) in these envelope proteins, the putative GAG-binding site contains four residues that are dissimilar in the two viruses, K395, T397, S403, and K409 in ZIKV E and Q386, K388, K394, and Q400 in DENV E. Identical acidic residues are located in both GAG-binding sites: D296 and E412 in ZIKV E and D290 and E403 in DENV E. When both GAG-binding sites (Figure S1) are considered, ZIKV E has a positive charge (with 13 basic and two acidic residues) lower than that of DENV E (with 14 basic and two acidic residues) at physiological pH, and this may help explain the 10-fold higher GAG binding affinity of DENV compared to that of ZIKV E. However, nonbasic or acidic residues can also have an impact on the specificity and affinity of GAG binding. A recent study suggests that examining the presence of asparagine and glutamine in addition to arginine and lysine in GAG-binding sites can allow better prediction of specificity and binding avidity for GAG-binding proteins.[84] In the positions where basic residues are missing in DENV E, glutamines and asparagine are present, Q293, Q386, N390, and Q400; in contrast, ZIKV E has no glutamines or asparagines at these sites.

After establishing that ZIKV E has a high affinity for HP, we investigated whether ZIKV E–GAG interaction exhibited structural specificity. In ZIKV's closely related cousin DENV, only longer chain length heparin oligosaccharides (dp10) effectively bind to DENV E and inhibit binding of DENV E to Vero cells.[47] A SPR competition assay was performed to determine whether ZIKV E also possesses this structural specificity in GAG binding. Although inhibition was negligible for smaller HP oligosaccharides (from dp4 to dp6), the level of inhibition increased to 18.6% for dp8 and to 89.2% for dp18. These results suggest that the minimum chain length of the HP oligosaccharide to efficiently occupy the GAG-binding site on ZIKV E may be dp8 and that it prefers an even longer chain length. These findings establish that ZIKV E–GAG interactions exhibit structural specificity in terms of chain length requirement.

In addition to chain length specificity, sulfation position and saccharide sequence affect efficient binding to GAGs and, thus, successful host cell invasion in various infectious agents, including parasites, i.e., *Plasmodium falciparum,* bacteria, i.e., *Helicobacter pylori,* and flaviviruses, i.e., DENV.[47,53,85] We screened various natural GAGs for their inhibition activity against HP–ZIKV E interactions to determine if ZIKV E–GAG interaction also showed this structural specificity. If the saccharide sequence and/or sulfation pattern did not play a role in GAG–ZIKV E interactions, ZIKV E would prefer binding to more sulfated GAGs and follow this trend: HP > CSD and CSE > KS > HS > CSA, CSB, and CSC.

However, the ZIKV E–GAG binding trend obtained from the competition assay is as follows: HP > CSE > CSB > HS > KS > CSD > CSA > CSC. These results suggest that ZIKV E–GAG binding also exhibits specific saccharide sequences and/or sulfation patterns like other pathogen–GAG interactions.

After learning that ZIKV E's interaction with GAGs exhibits structural specificity, we screened GAGs from human placenta tissues for their affinity for ZIKV E. ZIKV has been reported to cross the placental barrier and found in amniotic fluid of pregnant women at 28 weeks.[32] A recent study also reported that ZIKV infected placenta in the early development stage of pregnancy in mice.[33] Before infecting the fetus to cause anomalies, such as microcephaly, ZIKV first must strategically invade placental tissues. We isolated GAGs from human placenta and further processed them into CS and HS to identify GAGs that may mediate ZIKV's host cell entry. Disaccharide composition analysis shows that placenta largely consisted of CS (69.87%), HS (15.38%), and HA (14.75%) (Table 2). Because pathogens generally utilize GAGs as attachment factors to concentrate themselves on the surface of host cells and CS is the major component in placenta, we suspected that CS may be the main GAG-binding ZIKV E. The percent composition of placental CS shows that CSA and CSB (69%) and CSC (27.1%) were the main CS in placenta. It is notable that CSB was the GAG that bound third most strongly to ZIKV E from the competition assay. We also analyzed the disaccharide composition of placental HS, which was composed of 0S (50.7%), NS (24.9%), and NS2S (13.3%). We generated globally fit sensorgrams and calculated kinetic constants from injection of 500–3000 nM ZIKV E over placental CS- and HS-immobilized sensor chips (Figure 6 and Table 1). CS showed concentration-dependent binding at nanomolar concentrations of ZIKV E compared to HS-dependent binding. These results suggest that placental CS, possibly CSB, may be the GAG receptor that mediates placental cell entry of ZIKV.

Finally, we investigated if brain GAGs could mediate the neural cell entry of ZIKV. The SPR binding assay was performed to test ZIKV E's binding affinity for porcine brain CS- and HS-immobilized sensor chips. Brain HS showed concentration-dependent binding, and its sensorgrams showed a good fit to a Langmuir kinetic model. While placental and brain HS are both composed of two main types of HS (0S and NS2S), they differ in that placental HS contains NS and brain HS contains significant amounts of Tris and NS6S. "Fishing" experiments in which we screened a library of HS decasaccharides showed that HS decasaccharides that bound tightly to ZIKV E were enriched with TriS and 6S and not enriched with 0S. Porcine brain HS is composed of 60% 0S and 25% TriS and has only very small amounts of 6S. This may explain the weaker binding of porcine brain HS to ZIKV E when compared to that of placental CS. However, the HS composition varies across different organisms, and this HS came from a pig not a human. Moreover, the HS composition changes during brain development within an organism. Thus, it will be important to examine human HS taken from the human brain at early stages of development.

There are several established biological approaches to test whether cells without GAGs can bind envelope protein or be infected with ZIKV. Cells could be grown either in low-sulfate medium or in the presence of sodium chlorate to decrease the level of GAG sulfation.[47,86,87] Cells could be treated with GAG lyases to remove specific GAGs from the surface of cells.

[86,87] GAG biosynthesis could be blocked in knockout cell lines [i.e., Chinese hamster ovary (CHO) cells such as pgsD-618, pgsD-677, and pgsA-745].[47,86-88] While our study uses a biochemical method to demonstrate the interaction between GAGs and ZIKV E, *in vitro* cell-based studies relying on GAG-deficient cells will be needed to validate the importance of this binding for ZIKV infection.

Since the WHO declared Public Health Emergency of International Concern on ZIKV's ability to cause severe birth defects, many academic, government, and industry groups have been in a race to better understand the pathogenesis of ZIKV and to develop new detection methods and therapeutic approaches. DNA-based vaccines from Inovio and the National Institute of Allergy and Infectious Disease (NIAID) entered phase I clinical trials in August 2016. As promising as this is, it may still take several years until a safe and effective vaccine is available to combat ZIKV. DENV, a close relative to ZIKV, annually puts 2.5 billion people at risk and infects 20 million people. The development of a vaccine for DENV has been extremely challenging because of immunological interactions between the serotypes of DENV and immune enhancement of disease.[89] The first DENV vaccine, approved in Mexico in late 2015 and now in five more countries, has been reported to be ineffective among children who are at major risk of infection. This DENV vaccine also may cause more serious "secondary" infection depending on the transmission setting. Similar challenges might slow the development of a ZIKV vaccine. The current findings about the role of GAGs in ZIKV's host cell entry contribute to our understanding of ZIKV pathogenesis and might facilitate the development of detection and therapeutic approaches.[90]

In this study, we established that ZIKV envelope protein interacts with GAGs through electrostatic interactions and that specific chain lengths, saccharide sequences, and sulfation patterns are important in the binding of GAG to ZIKV E. Placental CS was identified as a candidate coreceptor for ZIKV E and may mediate host cell entry of ZIKV into the placenta. Studies of porcine brain HS show a concentration-dependent binding to ZIKV E, and "fishing" experiments suggest that HS with a higher TriS and 6S composition exhibits a higher affinity for ZIKV E. These findings begin to set a foundation needed to advance our understanding of the pathogenesis of ZIKV and should provide insight into the development of therapeutics for ZIKV.

Supplementary Material

Refer to Web version on PubMed Central for supplementary material.

Acknowledgments

Funding

This research was funded through National Institutes of Health Grants HL094463, HL62244, and NS088496.

ABBREVIATIONS

CSA	chondroitin sulfate A
CSB	chondroitin sulfate B

CSC	chondroitin sulfate C
CSD	chondroitin sulfate D
CSE	chondroitin sulfate E
DENV	Dengue virus
DENV E	Dengue virus envelope protein
dp	degree of polymerization
GAG	glycosaminoglycan
HP	heparin
HS	heparan sulfate
HA	hyaluronan
ITC	isothermal titration calorimetry
JEV	Japanese encephalitis virus
KS	keratan sufate
MEV	Murray encephalitis virus
PDB	Protein Data Bank
SA	streptavidin
SPR	surface plasmon resonance
TBEV	tick-borne encephalitis virus
WNV	West Nile virus
YFV	yellow fever virus
ZIKV	Zika virus
ZIKV E	Zika virus envelope protein

REFERENCES

(1). World health report insect-borne diseases (2016) World Health Organization, Geneva, http://www.who.int/mediacentre/factsheets/fs387/en/ (accessed October 5, 2016).

(2). WHO Director-General summarizes the outcome of the Emergency Committee regarding clusters of microcephaly and Guillain-barré syndrome (2016) World Health Organization, Geneva, http://www.who.int/mediacentre/news/statements/2016/emergency-committee-zika-microcephaly/en/ (accessed October 5, 2016).

(3). Dick G, Kitchen S, and Haddow A (1952) Zika Virus (I). Isolations and Serological Specificity. Trans. R. Soc. Trop. Med. Hyg 46, 509–520. [PubMed: 12995440]

(4). Cao-Lormeau V-M, Blake A, Mons S, Lastère S, Roche C, Vanhomwegen J, Dub T, Baudouin L, Teissier A, Larre P, Vial A-L, Decam C, Choumet V, Halstead SK, Willison HJ, Musset l ,

Manuguerra J-C, Despres P, Fournier E, Mallet H-P, Musso D, Fontanet A, Neil J, and Ghawché F (2016) Guillain-Barré Syndrome outbreak associated with Zika virus infection in French Polynesia: a case-control study. Lancet 387, 1531–1539. [PubMed: 26948433]

(5). Rozé B, Najioullah F, Fergé J-L, Apetse K, Brouste Y, Cesaire R, Fagour C, Fagour L, Hochedez P, Jeannin S, Joux J, Mehdaoui H, Valentino R, Signate A, and Cabié A (2016) Zika virus detection in urine from patients with Guillain-Barré syndrome on Martinique, January 2016. Euro Surveillance 21 (9), 1–4.

(6). Schuler-Faccini L, Ribeiro EM, Feitosa IML, Horovitz DDG, Cavalcanti DP, Pessoa A, Doriqui MJR, Neri JI, de Pina Neto JM, Wanderley HYC, Cernach M, El-Husny AS, Pone MVS, Serao CLC, and Sanseverino MTV (2016) and Brazilian Medical Genetics Society–Zika Embryopathy Task Force. (2016) Possible Association Between Zika Virus Infection and Microcephaly - Brazil. Morbidity and Mortality Weekly Report 65, 59–62. [PubMed: 26820244]

(7). Cauchemez S, Besnard M, Bompard P, Dub T, Guillemette-Artur P, Eyrolle-Guignot D, Salje H, Van Kerkhove MD, Abadie V, Garel C, Fontanet A, and Mallet HP (2016) Association between Zika virus and microcephaly in French Polynesia, 2013–15: A retrospective study. Lancet 387, 2125–2132. [PubMed: 26993883]

(8). Ventura CV, Maia M, Bravo-Filho V, Góis AL, and Belfort R (2016) Zika virus in Brazil and macular atrophy in a child with microcephaly. Lancet 387, 228.

(9). de Paula Freitas B, de Oliveira Dias JRJ, Prazeres J, Sacramento GAG, Ko AI, Maia MM, and Belfort RJ (2016) Ocular Findings in Infants With Microcephaly Associated With Presumed Zika Virus Congenital. JAMA Ophthalmol 134, 529–535. [PubMed: 26865554]

(10). Situation Report Zika Virus Microcephaly Guillain-Barré Syndrome (2016) World Health Organization, Geneva, http://www.who.int/emergencies/zika-virus/situation-report/en/ (accessed December 8, 2016).

(11). Pregnant Women with Any Laboratory Evidence of Possible Zika Virus Infection in the United States and Territories, 2016 (2016) Centers for Disease Control and Prevention, Atlanta,https://www.cdc.gov/zika/geo/pregwomen-uscases.html (accessed December 8, 2016).

(12). Chan JFW, Choi GKY, Yip CCY, Cheng VCC, and Yuen KY (2016) Zika fever and congenital Zika syndrome: An unexpected emerging arboviral disease. J. Infect 72, 507–524. [PubMed: 26940504]

(13). Besnard M, Lastère S, Teissier A, Cao-Lormeau VM, and Musso D (2014) Evidence of perinatal transmission of zika virus, French Polynesia, December 2013 and February 2014. Euro Surveillance 19, 20751. [PubMed: 24721538]

(14). Deckard DT, Chung WM, Brooks JT, Smith JC, Woldai S, Hennessey M, Kwit N, and Mead P (2016) Male-to-Male Sexual Transmission of Zika Virus - Texas, January 2016. MMWR Morb Mortal Wkly Rep 65, 372–374. [PubMed: 27078057]

(15). Venturi G, Zammarchi L, Fortuna C, Remoli ME, Benedetti E, Fiorentini C, Trotta M, Rizzo C, Mantella A, Rezza G, and Bartoloni A (2016) An autochthonous case of Zika due to possible sexual transmission, Florence, Italy, 2014. Euro Surveillance 21, 1–4.

(16). Foy BD, Kobylinski KC, Foy JLC, Blitvich BJ, Travassos da Rosa A, Haddow AD, Lanciotti RS, and Tesh RB (2011) Probable Non-Vector-borne Transmission of Zika Virus, Colorado, USA. Emerging Infect. Dis 17, 880–882.

(17). Motta IJF, Spencer BR, Cordeiro da Silva SG, Arruda MB, Dobbin JA, Gonzaga YBM, Arcuri IP, Tavares RCBS , Atta EH, Fernandes RFM, Costa DA, Ribeiro LJ, Limonte F, Higa LM, Voloch CM, Brindeiro RM, Tanuri A, and Ferreira OC (2016) Evidence for Transmission of Zika Virus by Platelet Transfusion. N. Engl J. Med 375, 1101–1103. [PubMed: 27532622]

(18). Hamel R, Dejarnac O, Wichit S, Ekchariyawat P, Neyret A, Luplertlop N, Perera-Lecoin M, Surasombatpattana P, Talignani L, Thomas F, Cao-Lormeau V-M, Choumet V, Briant L, Desprès P, Amara A, Yssel H, and Missé D (2015) Biology of Zika Virus Infection in Human Skin Cells. J. Virol 89, 8880–8896. [PubMed: 26085147]

(19). Tang H, Hammack C, Ogden SC, Wen Z, Qian X, Li Y, Yao B, Shin J, Zhang F, Lee EM, Christian KM, Didier RA, Jin P, Song H, and Ming G-L (2016) Zika Virus Infects Human Cortical Neural Progenitors and Attenuates Their Growth. Cell Stem Cell 18, 587–590. [PubMed: 26952870]

(20). Qian X, Nguyen HN, Song MM, Hadiono C, Ogden SC, Hammack C, Yao B, Hamersky GR, Jacob F, Zhong C, Yoon KJ, Jeang W, Lin L, Li Y, Thakor J, Berg DA, Zhang C, Kang E, Chickering M, Nauen D, Ho CY, Wen Z, Christian KM , Shi PY, Maher BJ, Wu H, Jin P, Tang H, Song H, and Ming GL (2016) Brain-Region-Specific Organoids Using Minibioreactors for Modeling ZIKV Exposure. Cell 165, 1238–1254. [PubMed: 27118425]

(21). Soares de Oliveira-Szejnfeld P, Levine D, de Oliveira Melo AS, Amorim MMR, Batista AG, Chimelli L, Tanuri A, Aguiar RS,Malinger G, Ximenes R, Robertson R, Szejnfeld J, and Tovar-Moll F (2016) Congenital Brain Abnormalities and Zika Virus: What the Radiologist Can Expect to See Prenatally and Postnatally. Radiology 281, 203–218. [PubMed: 27552432]

(22). Lazear HM, Govero J, Smith AM, Platt DJ, Fernandez E, Miner JJ, and Diamond MS (2016) A Mouse Model of Zika Virus Pathogenesis. Cell Host Microbe 19, 720–730. [PubMed: 27066744]

(23). Miner JJ, Cao B, Govero J, Smith AM, Fernandez E, Cabrera OH, Garber C, Noll M, Klein RS, Noguchi KK, Mysorekar IU, and Diamond MS (2016) Zika Virus Infection during Pregnancy in Mice Causes Placental Damage and Fetal Demise. Cell 165, 1081–1091. [PubMed: 27180225]

(24). Nowakowski TJ, Pollen AA, Di Lullo E, Sandoval-Espinosa C, Bershteyn M, and Kriegstein AR (2016) Expression Analysis Highlights AXL as a Candidate Zika Virus Entry Receptor in Neural Stem Cells. Cell Stem Cell 18, 591–596. [PubMed: 27038591]

(25). Morrison C (2016) DNA vaccines against Zika virus speed into clinical trials. Nat. Rev. Drug Discovery 15, 521–522. [PubMed: 27469223]

(26). Reyes-del Valle J, Chavez-Salinas S, Medina F, and del Angel RM (2005) Heat Shock Protein 90 and Heat Shock Protein 70 Are Components of Dengue Virus Receptor Complex in Human Cells. J. Virol 79, 4557–4567. [PubMed: 15795242]

(27). Aoki C, Hidari KIPJ, Itonori S, Yamada A, Takahashi N , Kasama T, Hasebe F, Islam MA, Hatano K, Matsuoka K, Taki T, Guo CT, Takahashi T, Sakano Y, Suzuki T, Miyamoto D, Sugita M, Terunuma D, Morita K, and Suzuki Y (2006) Identification and characterization of carbohydrate molecules in mammalian cells recognized by dengue virus type 2. J. Biochem 139, 607–614. [PubMed: 16567427]

(28). Chen YC, Wang SY, and King CC (1999) Bacterial lipopolysaccharide inhibits dengue virus infection of primary human monocytes/macrophages by blockade of virus entry via a CD14-dependent mechanism. J. Virol 73, 2650–2657. [PubMed: 10074110]

(29). Jindadamrongwech S, Thepparit C, and Smith DR (2004) Identification of GRP 78 (BiP) as a liver cell expressed receptor element for dengue virus serotype 2. Arch. Virol 149, 915–927. [PubMed: 15098107]

(30). Thepparit C, and Smith DR (2004) Serotype-specific entry of dengue virus into liver cells: identification of the 37-kilodalton/67-kilodalton high-affinity laminin receptor as a dengue virus serotype 1 receptor. J. Virol 78, 12647–12656. [PubMed: 15507651]

(31). Lozach PY, Burleigh L, Staropoli I, Navarro-Sanchez E, Harriague J, Virelizier JL, Rey FA, Desprès P, Arenzana-Seisdedos F, and Amara A (2005) Dendritic cell-specific intercellular adhesion molecule 3-grabbing non-integrin (DC-SIGN)-mediated enhancement of dengue virus infection is independent of DC-SIGN internalization signals. J. Biol. Chem 280, 23698–23708. [PubMed: 15855154]

(32). Navarro-Sanchez E, Altmeyer R, Amara A, Schwartz O, Fieschi F, Virelizier JL, Arenzana-Seisdedos F, and Despres P (2003) Dendritic-cell-specific ICAM3-grabbing non-integrin is essential for the productive infection of human dendritic cells by mosquitocell-derived dengue viruses. EMBO Rep. 4, 723–728. [PubMed: 12783086]

(33). Tassaneetrithep B, Burgess TH, Granelli-Piperno A, Trumpfheller C, Finke J, Sun W, Eller MA, Pattanapanyasat K, Sarasombath S, Birx DL, Steinman RM, Schlesinger S, and Marovich MA (2003) DC-SIGN (CD209) mediates dengue virus infection of human dendritic cells. J. Exp. Med 197, 823–829. [PubMed: 12682107]

(34). Miller JL, deWet BJM, Martinez-Pomares L, Radcliffe CM, Dwek RA, Rudd PM, and Gordon S (2008) The Mannose Receptor Mediates Dengue Virus Infection of Macrophages. PLoS Pathog. 4, e17. [PubMed: 18266465]

(35). Chen S-T, Lin Y-L, Huang M-T, Wu M-F, Cheng S-C, Lei H-Y, Lee C-K, Chiou T-W, Wong C-H, and Hsieh S-L (2008) CLEC5A is critical for dengue-virus-induced lethal disease. Nature 453, 672–676. [PubMed: 18496526]

(36). Mercado-Curiel RF, Esquinca-Avilés HA, Tovar R, Díaz-Badillo A, Camacho-Nuez M, and de Lourdes Munoz M (2006) The four serotypes of dengue recognize the same putative receptors in Aedes aegypti midgut and Ae. albopictus cells. BMC Microbiol. 6, 85. [PubMed: 17014723]

(37). Yazi Mendoza M, Salas-Benito JS, Lanz-Mendoza H, Hernández-Martinez S, and Del Angel RM (2002) A putative receptor for dengue virus in mosquito tissues: Localization of a 45-KDA glycoprotein. Am. J. Trop. Med. Hyg 67, 76–84. [PubMed: 12363068]

(38). Pokidysheva E, Zhang Y, Battisti AJ, Bator-Kelly CM, Chipman PR, Xiao C, Gregorio GG, Hendrickson WA, Kuhn RJ, and Rossmann MG (2006) Cryo-EM reconstruction of dengue virus in complex with the carbohydrate recognition domain of DC-SIGN. Cell 124, 485–493. [PubMed: 16469696]

(39). Davis CW, Nguyen H-Y, Hanna SL, Sánchez MD, Doms RW, and Pierson TC (2006) West Nile virus discriminates between DC-SIGN and DC-SIGNR for cellular attachment and infection. J. Virol 80, 1290–301. [PubMed: 16415006]

(40). Davis CW, Mattei LM, Nguyen HY, Ansarah-Sobrinho C, Doms RW, and Pierson TC (2006) The location of asparagine-linked glycans on West Nile virions controls their interactions with CD209 (dendritic cell-specific ICAM-3 grabbing nonintegrin). J. Biol. Chem 281, 37183–37194. [PubMed: 17001080]

(41). Chu JJH, and Ng ML (2004) Interaction of West Nile virus with $\alpha_V\beta_3$ integrin mediates virus entry into cells. J. Biol. Chem 279, 54533–54541. [PubMed: 15475343]

(42). Lee JW-M, Chu JJ-H, and Ng M-L (2006) Quantifying the specific binding between West Nile virus envelope domain III protein and the cellular receptor alphaVbeta3 integrin. J. Biol. Chem 281, 1352–1360. [PubMed: 16275649]

(43). Medigeshi GR, Hirsch AJ, Streblow DN, Nikolich-Zugich J, and Nelson JA (2008) West Nile virus entry requires cholesterol-rich membrane microdomains and is independent of $\alpha v\beta 3$ integrin. J. Virol 82, 5212–5219. [PubMed: 18385233]

(44). van der Schaar HM, Rust MJ, Chen C, van der Ende-Metselaar H, Wilschut J, Zhuang X, and Smit JM (2008) Dissecting the cell entry pathway of dengue virus by single-particle tracking in living cells. PLoS Pathog. 4, e1000244. [PubMed: 19096510]

(45). Ishak R, Tovey DG, and Howard CR (1988) Morphogenesis of yellow fever virus 17D in infected cell cultures. J. Gen. Virol 69 (Part 2), 325–335. [PubMed: 3339329]

(46). Nawa M, Takasaki T, Yamada KI, Kurane I, and Akatsuka T (2003) Interference in Japanese encephalitis virus infection of Vero cells by a cationic amphiphilic drug, chlorpromazine. J. Gen. Virol 84, 1737–1741. [PubMed: 12810867]

(47). Chen Y, Maguire T, Hileman RE, Fromm JR, Esko JD, Linhardt RJ, and Marks RM (1997) Dengue virus infectivity depends on envelope protein binding to target cell heparan sulfate. Nat. Med 3, 866–871. [PubMed: 9256277]

(48). Germi R, Crance J-M, Garin D, Guimet J, Lortat-Jacob H, Ruigrok RWH, Zarski J-P, and Drouet E (2002) Heparan Sulfate-Mediated Binding of Infectious Dengue Virus Type 2 and Yellow Fever Virus. Virology 292, 162–168. [PubMed: 11878919]

(49). Hilgard P (2000) Heparan Sulfate Proteoglycans Initiate Dengue Virus Infection of Hepatocytes. Hepatology 32, 1069–1077. [PubMed: 11050058]

(50). Chen HL, Her SY, Huang KC, Cheng HT, Wu CW, Wu SC, and Cheng JW (2010) Identification of a heparin binding peptide from the Japanese encephalitis virus envelope protein. Biopolymers 94, 331–338. [PubMed: 20069543]

(51). Lee E, and Lobigs M (2008) E protein domain III determinants of yellow fever virus 17D vaccine strain enhance binding to glycosaminoglycans, impede virus spread, and attenuate virulence. J. Virol 82, 6024–33. [PubMed: 18400851]

(52). Mandl CW, Kroschewski H, Allison SL, Kofler R, Holzmann H, Meixner T, and Heinz FX (2001) Adaptation of Tick-Borne Encephalitis Virus to BHK-21 Cells Results in the Formation of Multiple Heparan Sulfate Binding Sites in the Envelope Protein and Attenuation In Vivo Adaptation of Tick-Borne Encephalitis Virus to BHK-21 Cells Results in the Forma. J. Virol 75, 5627–5637. [PubMed: 11356970]

(53). Maier AG, Cooke BM, Cowman AF, and Tilley L (2009) Malaria parasite proteins that remodel the host erythrocyte. Nat. Rev. Microbiol 7, 341–354. [PubMed: 19369950]

(54). Boyle KA, and Compton T (1998) Receptor-binding properties of a soluble form of human cytomegalovirus glycoprotein B. J. Virol 72, 1826–1833. [PubMed: 9499033]

(55). Patel M, Yanagishita M, Roderiquez G, Bou-Habib DC, Oravecz T, Hascall VC, and Norcross MA (1993) Cell-surface heparan sulfate proteoglycan mediates HIV-1 infection of T cell lines. AIDS Res. Hum. Retroviruses 9, 167–174. [PubMed: 8096145]

(56). Jenssen H, Sandvik K, Andersen JH, Hancock REW, and Gutteberg TJ (2008) Inhibition of HSV cell-to-cell spread by lactoferrin and lactoferricin. Antiviral Res. 79, 192–198. [PubMed: 18456345]

(57). Kamhi E, Joo EJ, Dordick JS, and Linhardt RJ (2013) Glycosaminoglycans in infectious disease. Biol. Rev 88, 928–943. [PubMed: 23551941]

(58). Linhardt RJ, and Toida T (2004) Role of glycosaminoglycans in cellular communication. Acc. Chem. Res. 37, 431–438. [PubMed: 15260505]

(59). Sirohi D, Chen Z, Sun L, Klose T, Pierson T, Rossmann M, and Kuhn R (2016) The 3.8 Å resolution cryo-EM structure of Zika virus. Science 352 (6284), 467–470. [PubMed: 27033547]

(60). Kostyuchenko V, Lim E, Zhang S, Fibriansah G, Ng T, Ooi J, Shi J, and Lok S (2016) Structure of the thermally stable Zika virus. Nature 533, 425–428. [PubMed: 27093288]

(61). Dai L, Song J, Lu X, Deng Y, Musyoki A, Cheng H, Zhang Y, Yuan Y, Song H, Haywood J, Xiao H, Yan J, Shi Y, Qin C, Qi J, and Gao G (2016) Structures of the Zika Virus Envelope Protein and Its Complex with a Flavivirus Broadly Protective Antibody. Cell Host Microbe 19 (5), 696–704. [PubMed: 27158114]

(62). Zhang X, Ge P, Yu X, Brannan J, Bi G, Zhang Q, Schein S, and Zhou Z (2013) Cryo-EM structure of the mature dengue virus at 3.5-Å resolution. Nat. Struct. Mol. Biol. 20, 105–110. [PubMed: 23241927]

(63). Nybakken G, Nelson C, Chen B, Diamond M, and Fremont D (2006) Crystal structure of the West Nile virus envelope glycoprotein. J. Virol 80 (23), 11467–11474. [PubMed: 16987985]

(64). Sánchez IJ, and Ruiz BH (1996) A single nucleotide change in the E protein gene of dengue virus 2 Mexican strain affects neurovirulence in mice. J. Gen. Virol 77, 2541–2545. [PubMed: 8887488]

(65). Lin B, Parrish CR, Murray JM, and Wright PJ (1994) Localization of a neutralizing epitope on the envelope protein of Dengue Virus Type 2. Virology 202, 885–890. [PubMed: 7518164]

(66). Jiang WR, Lowe A, Higgs S, Reid H, and Gould EA (1993) Single amino acid codon changes detected in louping ill virus antibody-resistant mutants with reduced neurovirulence. J. Gen. Virol 74, 931–935. [PubMed: 8388021]

(67). Jennings AAD, Gibson CA, Miller BR, Mathews JH, Mitchell CJ, Roehrig JT, Wood DJ, Taffs F, Sil BK, Whitby SN, Whitby JE, Monath TP, Minor PD, Sanders PG, and Barrett ADT (1994) Analysis of a Yellow Fever Virus Isolated from a Fatal Case of Vaccine-Associated Human Encephalitis. J. Infect. Dis 169, 512–518. [PubMed: 7908925]

(68). Holzmann H, Heinz FX, Mandl CW, Guirakhoo F, and Kunz C (1990) A single amino acid substitution in envelope protein E of tick-borne encephalitis virus leads to attenuation in the mouse model. J. Virol 64, 5156–5159. [PubMed: 2398538]

(69). Weyers A, Yang B, Solakyildirim K, Yee V, Li L, Zhang F, and Linhardt RJ (2013) Isolation of bovine corneal keratan sulfate and its growth factor and morphogen binding. FEBS J. 280, 2285–2293. [PubMed: 23402351]

(70). Pervin A, Gallo C, Jandik KA, Han X-J, and Linhardt RJ (1995) Preparation and structural characterization of large heparin-derived oligosaccharides. Glycobiology 5, 83–95. [PubMed: 7772871]

(71). Linhardt RJ, Turnbull JE, Wang HM, Loganathan D, and Gallagher JT (1990) Examination of the substrate specificity of heparin and heparan sulfate lyases. Biochemistry 29, 2611–2617. [PubMed: 2334685]

(72). Beaudet JM, Mansur L, Joo EJ, Kamhi E, Yang B, Clausen TM, Salanti A, Zhang F, and Linhardt RJ (2014) Characterization of human placental glycosaminoglycans and regional binding to VAR2CSA in malaria infected erythrocytes. Glycoconjugate J. 31, 109–116.

(73). Linhardt RJ, and Gunay NS (1999) Production and chemical processing of low molecular weight heparins. Semin. Thromb. Hemostasis 25, 5–11.

(74). Okamoto K, Kinoshita H, Parquet M. d.C. , Raekiansyah M, Kimura D, Yui K, Islam MA, Hasebe F, and Morita K (2012) Dengue virus strain DEN2 16681 utilizes a specific glycochain of syndecan-2 proteoglycan as a receptor. J. Gen. Virol 93, 761–770. [PubMed: 22170634]

(75). Kato D, Era S, Watanabe I, Arihara M, Sugiura N, Kimata K , Suzuki Y, Morita K, Hidari KIPJ, and Suzuki T (2010) Antiviral activity of chondroitin sulphate E targeting dengue virus envelope protein. Antiviral Res. 88, 236–243. [PubMed: 20851716]

(76). Ghosh T, Chattopadhyay K, Marschall M, Karmakar P, Mandal P, and Ray B (2009) Focus on antivirally active sulfated polysaccharides: From structure-activity analysis to clinical evaluation. Glycobiology 19, 2–15. [PubMed: 18815291]

(77). Gama CI, Tully SE, Sotogaku N, Clark PM, Rawat M, Vaidehi N, Goddard WA, Nishi A, and Hsieh-Wilson LC (2006) Sulfation patterns of glycosaminoglycans encode molecular recognition and activity. Nat. Chem. Biol 2, 467–473. [PubMed: 16878128]

(78). Liu Z, Masuko S, Solakyildirim K, Pu D, Linhardt RJ, and Zhang F (2010) Glycosaminoglycans of the porcine central nervous system. Biochemistry 49, 9839–9847. [PubMed: 20954748]

(79). Zhang F, Zhang Z, Lin X, Beenken A, Eliseenkova A, Mohammadi M, and Linhardt RJ (2009) Compositional analysis on heparin/heparan sulfate interacting with FGF•FGFR complexes. Biochemistry 48, 8379–8386. [PubMed: 19591432]

(80). Day YS, Baird CL, Rich RL, and Myszka DG (2002) Direct comparison of binding equilibrium, thermodynamic, and rate constants determined by surface- and solution-based biophysical methods. Protein Sci. 11 , 1017–1025. [PubMed: 11967359]

(81). Cardin AD, and Weintraub HJ (1989) Molecular modeling of protein-glycosaminoglycan interactions. Arterioscler., Thromb., Vasc. Biol 9, 21–32.

(82). Hileman RE, Fromm JR, Weiler JM, and Linhardt RJ (1998) Glycosaminoglycan-Protein Interaction: Definition of Con-sensus Sites in Glycosaminoglycan Binding Proteins. BioEssays 20, 156–167. [PubMed: 9631661]

(83). Hileman RE, Jennings RN, and Linhardt RJ (1998) Thermodynamic Analysis of Heparin Interaction with a Basic CyclicProtein Using Isothermal Titration Calorimetry. Biochemistry 37, 15231–15237. [PubMed: 9790687]

(84). Sarkar A, and Desai UR (2015) A Simple Method for Discovering Druggable, Specific Glycosaminoglycan-Protein Systems. Elucidation of Key Principles from Heparin/Heparan Sulfate-Binding Proteins. PLoS One 10 (10), e0141127. [PubMed: 26488293]

(85). Ascencio F, Fransson LA, and Wadstrom T (1993) Affinity of the gastric pathogen Helicobacter pylori for the N-sulphated glycosaminoglycan heparan sulphate. J. Med. Microbiol 38, 240–244. [PubMed: 7682621]

(86). Hilgard P, and Stockert R (2000) Heparan Sulfate Proteoglycans Initiate Dengue Virus Infection of Hepatocytes. Hepatology 32, 1069–1077. [PubMed: 11050058]

(87). Germi R, Crance J-M, Garin D, Guimet J, Lortat-Jacob H, Ruigrok RWH, Zarski J-P, and Drouet E (2002) Heparan Sulfate-Mediated Binding of Infectious Dengue Virus Type 2 and Yellow Fever Virus. Virology 292, 162–168. [PubMed: 11878919]

(88). Kroschewski H, Allison SL, Heinz FX, and Mandl CW (2003) Role of heparan sulfate for attachment and entry of tick-borne encephalitis virus. Virology 308, 92–100. [PubMed: 12706093]

(89). Ferguson NM, Rodríguez-Barraquer I, Dorigatti I, Mier-y-Teran-Romero L, Laydon DJ, and Cummings DAT (2016) Benefits and risks of the Sanofi-Pasteur dengue vaccine: Modeling optimal deployment. Science 353 (6303), 1033–1036. [PubMed: 27701113]

(90). Yachdav G, Wilzbach S, Rauscher B, Sheridan R, Sillitoe I, Procter J, Lewis S, Rost B, and Goldberg T (2016) MSAViewer: interactive JavaScript visualization of multiple sequence alignments. Bioinformatics 32 (22), 3501–3503. [PubMed: 27412096]

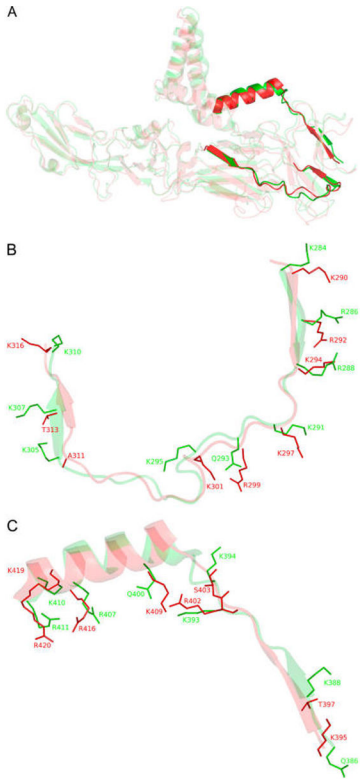

Figure 1.

(A) Full length structural alignment of ZIKV E (red, PDB entry 51RE) and DENV2 E (green, PDB entry 3J27). Bold structures are putative GAG-binding sites within the rest of the envelope proteins represented in more transparent structures. (B) Superimposition of putative GAG-binding site I of ZIKV E (K290–K316) and DENV2 E (K284–K310). Surface residues that may contribute to GAG binding are illustrated as sticks. (C) Putative GAG-binding site II of ZIKV E (R395–R420) and DENV2 E (Q386–R411) (see Figure S1 for a sequence alignment).

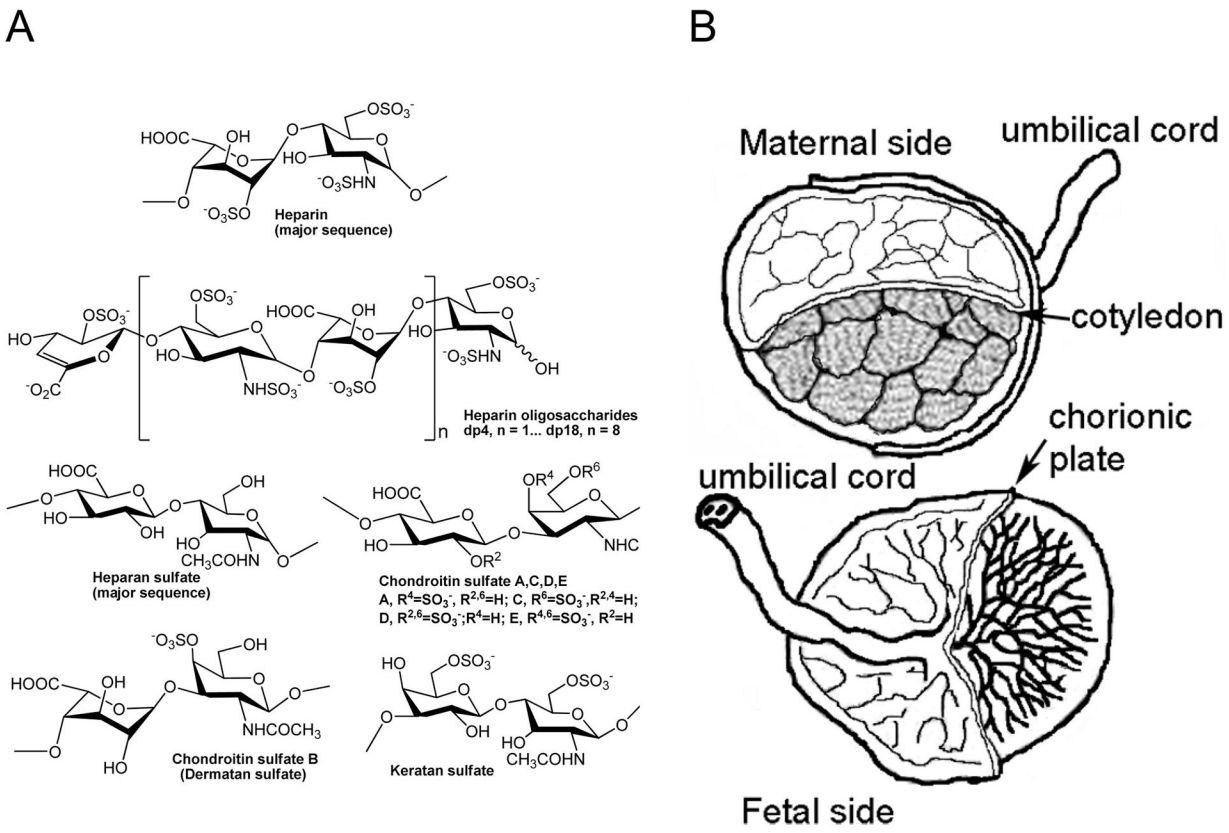

Figure 2.

(A) Chemical structures of various glycosaminoglycans and heparin oligosaccharides. (B) Portions of human placental tissues analyzed.

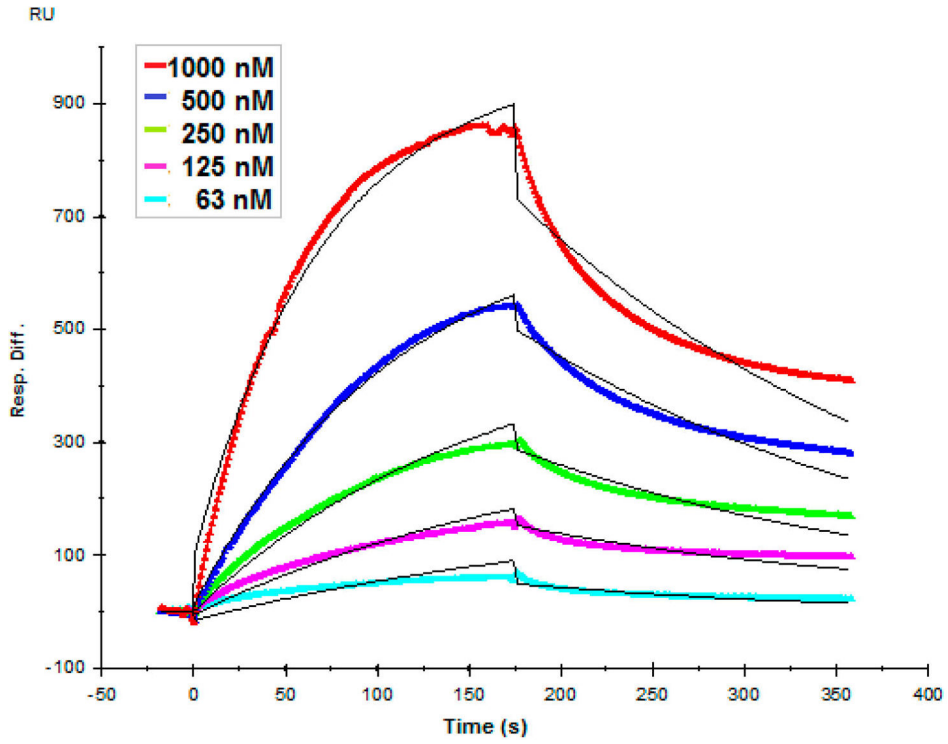

Figure 3.

Sensorgrams of interactions between ZIKV E protein and porcine intestinal heparin. ZIKV E (63, 125, 250, 500, and 1000 nM) was injected over the surface of immobilized heparin at a flow rate of 30 μL/min. The black curves are the fitting curves using models from BIAevaluation version 4.0.1.

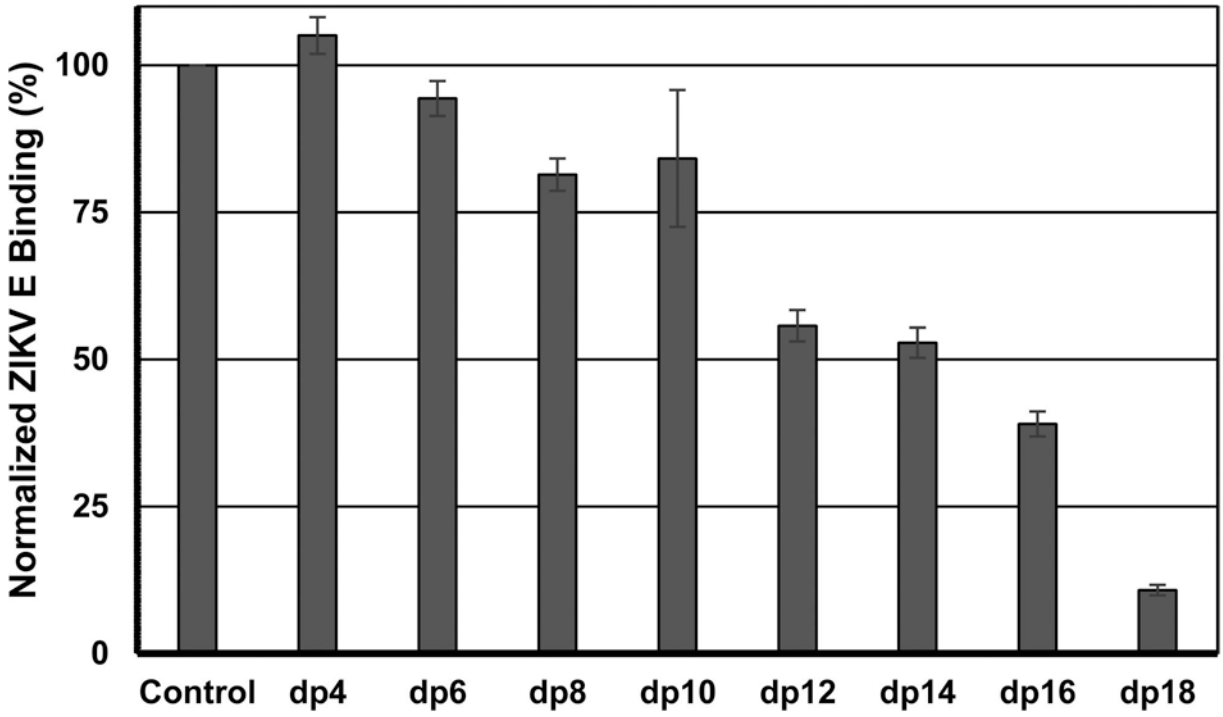

Figure 4.

Inhibition of binding of various chain length heparin oligosaccharides to ZIKV E–HP. A mixture of ZIKV E and HP oligosaccharides (dp2–dp18) was injected over the surface of immobilized heparin at a flow rate of 30 μL/min. Binding of ZIKV E to immobilized HP was normalized on the basis of the RU obtained from a negative control (HBS-EP buffer). The error bars are standard deviations from triplicate experiments.

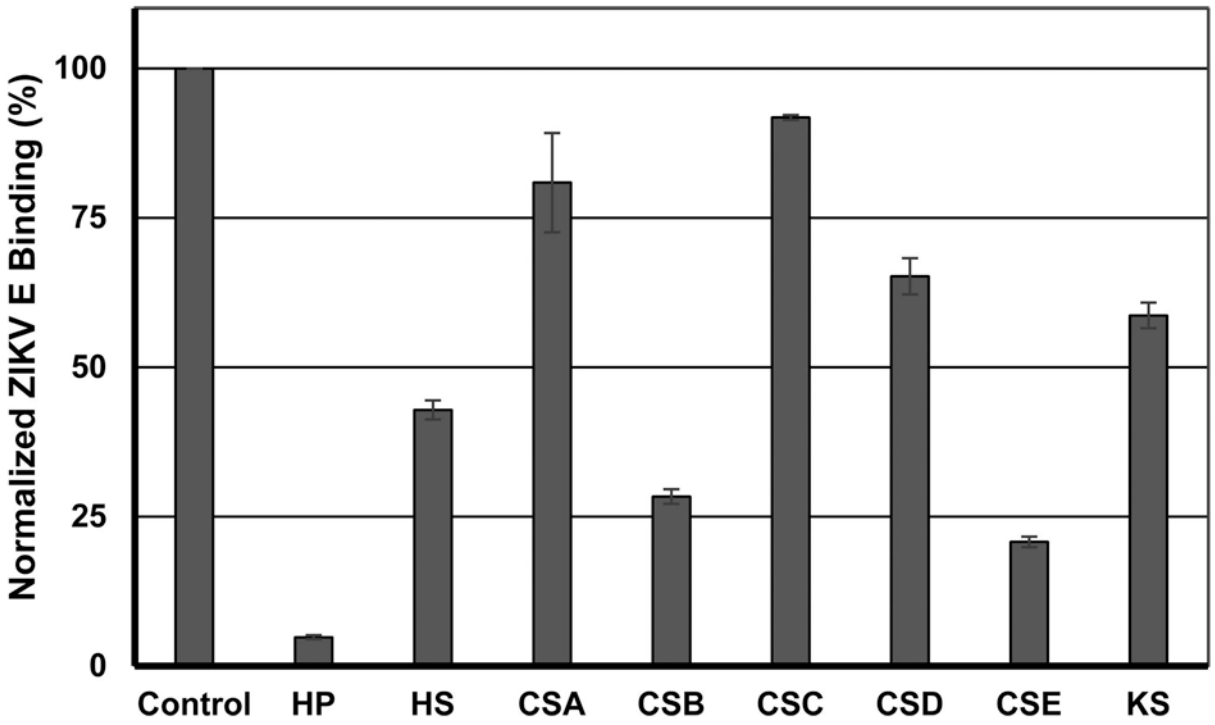

Figure 5.

Inhibition of binding of various natural GAGs to ZIKV E–HP. A mixture of ZIKV E and various GAGs (HP, HS, CSA, CSB, CSC, CSD, CSE, and KS) was injected over the surface of immobilized heparin at a flow rate of 30 μL/min. Binding of ZIKV E to immobilized HP was normalized on the basis of the RU obtained from a negative control (HBS-EP buffer). The error bars are standard deviations from triplicate experiments.

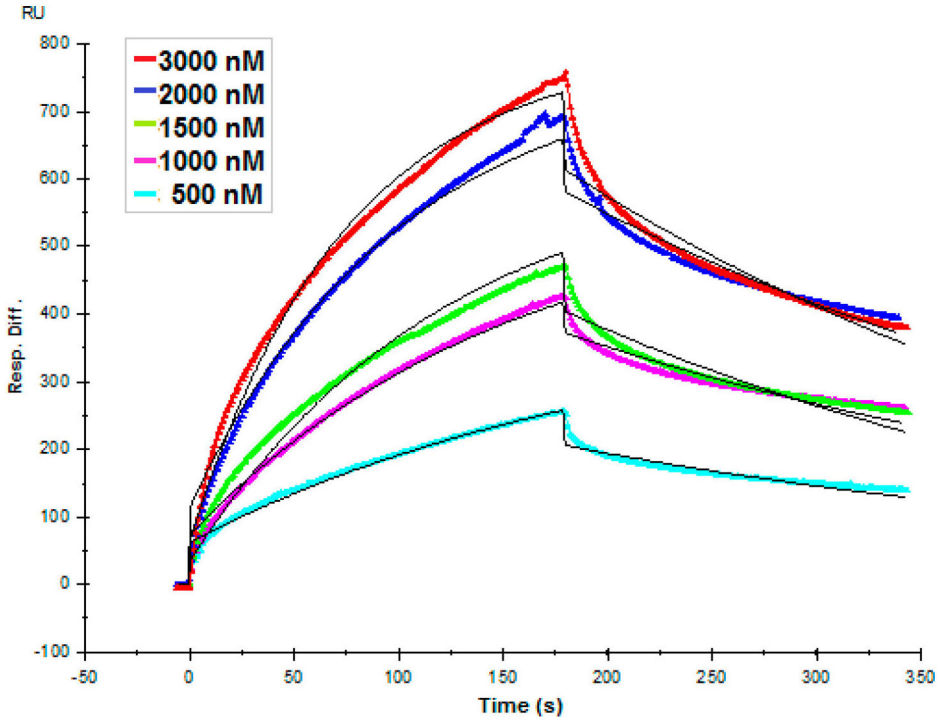

Figure 6.

Binding interactions between ZIKV E and placental CS. ZIKV E (500, 1000, 1500, 2000, and 3000 nM) was injected over the surface of immobilized human placental CS at a flow rate of 30 μL/min. The black curves are the fitting curves using models from BIAevaluation version 4.0.1.

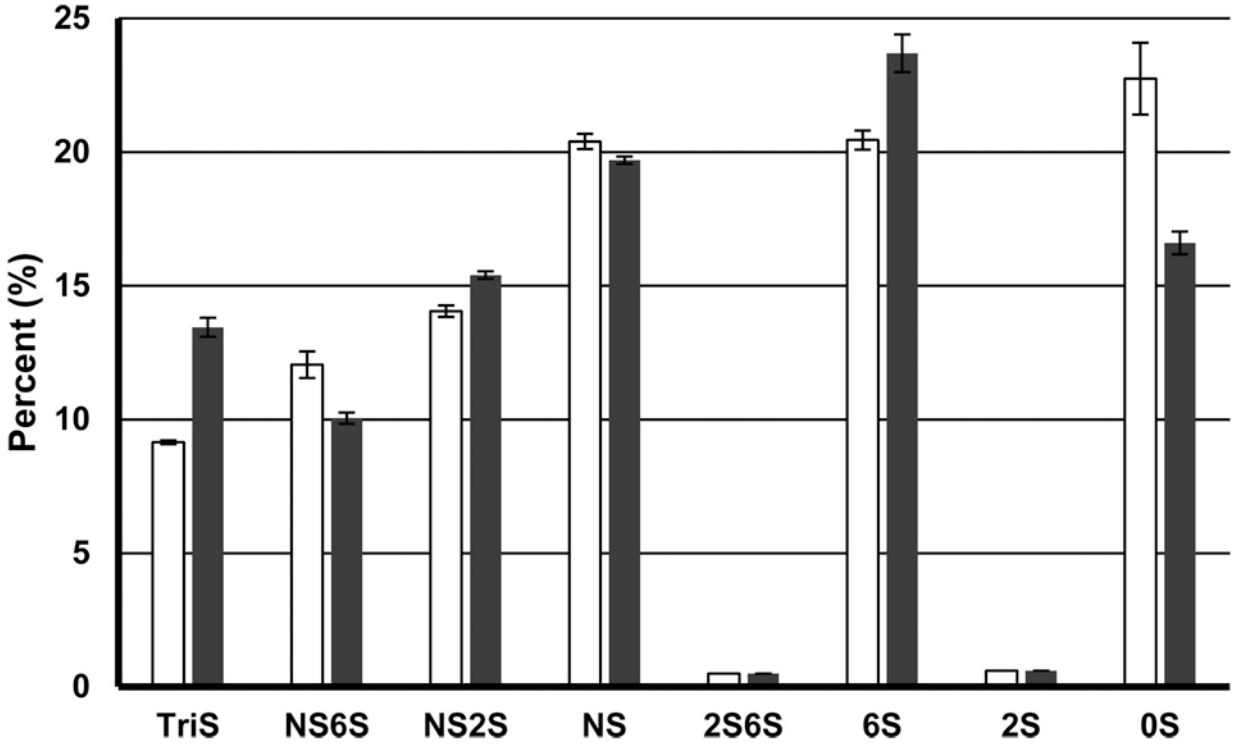

Figure 7.

"Fishing" experiments. The library of HS decasaccharides was screened to identify high-ZIKV E binding affinity components using LC–MS. White columns show data from the control, and black columns show data for GAGs bound to ZIKV E. The error bars are standard deviations from triplicate experiments.

Table 1.

Binding Kinetics of ZIKV E–GAG Interactions from SPR Binding Assays

	k_a (M^{-1} s^{-1})	k_d (s^{-1})	K_D (nM)
porcine intestinal HP	9.67×10^3[a] (±135)	$4.28 \times 10^{-3} \pm 4.6 \times 10^{-5}$	443
human placental HS	2.32×10^3 (±123)	$2.95 \times 10^{-3} \pm 4.9 \times 10^{-5}$	894
human placental CS	4.10×10^3 (±92)	$2.70 \times 10^{-3} \pm 1.5 \times 10^{-4}$	658
porcine brain HS	2.07×10^3 (±42)	$2.02 \times 10^{-3} \pm 8.2 \times 10^{-5}$	977
porcine brain CS	1.86×10^3 (±49)	$2.45 \times 10^{-3} \pm 1.4 \times 10^{-4}$	1310

[a]The values in parentheses are the standard deviations (SDs) from global fitting of five injections.

Table 2.

Disaccharide Analysis of Total Human Placental GAG via LC–MS[a]

	total GAG disaccharide composition (%)			
	C	**CH**	**UB**	**average**
CS	71.9	68.4	69.3	69.9 ± 1.8
HS	23.1	15.7	7.3	15.4 ± 7.9
HA	4.96	15.9	23.4	14.8 ± 9.3

[a]C is cotyledon, CH chorionic plate, and UB umbilical cord. The standard deviation was generated from differences between GAG compositions of three different regions.

Table 3.

Disaccharide Analysis of Human Placental CS and HS via LC–MS[a]

	CS disaccharide composition (%)					HS disaccharide composition (%)			
	C	**CH**	**UB**	**average**		**C**	**CH**	**UB**	**average**
TriS	0	0	0	0	TriS	3.6	4.4	0.5	2.8 ± 2.1
2S4S	0.9	0.7	0.5	0.7 ± 0.2	NS6S	4.7	6.1	3.7	4.8 ± 1.2
2S6S	0.8	0.7	0.6	0.7 ± 0.1	NS2S	7.2	14	19	13 ± 5.8
4S6S	0.2	0.6	0	0.3 ± 0.3	2S6S	0	0	0	0
6S	26	24	31	27 ± 3.6	NS	19	27	29	25 ± 5.0
4S	69	73	65	69 ± 3.7	6S	3	3.5	4	3.5 ± 0.5
2S	0	0	0	0	2S	0	0	0	0
0S	2.3	1.4	2.6	2.1 ± 0.6	0S	62	46	44	50.7 ± 10

[a]C is cotyledon, CH chorionic plate, and UB umbilical cord. The standard deviation was generated from differences among GAG compositions of three different regions. See Figure S3 for analytical error analysis.